Mutations in RBD of SARS-CoV-2 Omicron variant result stronger binding to human ACE2 protein

Cecylia S. Lupala[a], Yongjin Ye[a], Hong Chen[b], Xiao-dong Su[b,*]
Haiguang Liu[a,c,*],

[a]Complex Systems Division, Beijing Computational Science Research Center, Haidian, Beijing 100193, People's Republic of China
[b]School of Life Sciences, State Key Laboratory of Protein and Plant Gene Research and Biomedical Pioneering Innovation Center (BIOPIC), Peking University, Beijing 100871, People's Republic of China
[c]Physics Department, Beijing Normal University, Haidian, Beijing 100875, People's Republic of China

*Corresponding authors: Xiao-dong Su, xdsu@pku.edu.cn Or Haiguang Liu, hgliu@csrc.ac.cn

Abstract

The spreading of SARS-CoV-2 virus resulted the COVID-19 pandemic, which has caused more than 5 millions of death globally. Several major variants of SARS-CoV-2 have emerged and placed challenges in controlling the infections. The recently emerged Omicron variant raised serious concerns about reducing efficacy of antibodies or vaccines, due to its vast mutations. We modelled the complex structure of human ACE2 protein and the receptor binding domain of Omicron variant, then conducted atomistic molecular dynamics simulations to study the binding interactions. The analysis shows that the Omicron variant RBD binds more strongly to the human ACE2 protein than the original strain. The mutation at the ACE2-RBD interface enhanced the tight binding by increasing hydrogen bonding interaction and enlarging buried solvent accessible surface area.

Keywords: SARS-CoV-2, Omicron, ACE2, mutation, molecular dynamics simulation

Introduction

The COVID-19 pandemic caused by the SARS-CoV-2 is still affecting global health and economy seriously[1]. According to JHU CSSE COVID-19 Data[2], there are 266 million infections and over 5.26 million fatalities as of December 6, 2021. Several vaccines have been developed and applied to prevent the spreading of SARS-CoV-2 viruses[3], however, these efforts are challenged by emerged virus variants due to mutations [4–7]. Among major variants, several strains were called out to be 'variant of concerns (VOC)' by the world health organization (WHO). On November 26, 2021, the WHO named a new variant (B.1.1.529) to be Omicron, designated to be a VOC [8]. The Omicron variant has accumulated a vast number of mutations, particularly in spike proteins that are responsible for the initiation of infection, i.e., the cell entry. There are 15 mutations on the receptor binding domain (RBD) of the spike protein, which has over 30 mutations in total (see Figure 1) [8,9]. Such a large number of accumulated mutations is unprecedent. Because the spike protein is the target of many antibodies or drugs, it is crucial to investigate the impacts to the efficacy of neutralizing antibodies, under the concerns of immune escapes. Furthermore, about 10 mutations are at the RBD binding interface to the receptor protein, the Angiotensin converting enzyme 2 (ACE2)[10,11]. This level of mutation also raised a question whether the RBD of Omicron variant binds tightly to the ACE2, and whether there is an alternative receptor that facilitate the infection of healthy cells.

Computational modeling and dynamics simulations have been applied to investigate the interactions between the SARS-CoV-2 RBD and the ACE2 proteins [12,13]. Before the structures of RBD-ACE2 complex were resolved experimentally, homology modeling and simulations have successfully predicted the model and quantified the interactions [13,14]. Computer simulations were also used to study the interactions between RBD and ACE2 proteins from other mammals, and the results provide hints on molecular mechanism for

SARS-CoV-2 infection to other animals [15,16]. Here, we followed the same approach, constructed the structure of human ACE2 and the RBD of Omicron variant (denoted as ACE2-RBD^{O}, where the superscript indicates Omicron). Then the structure is subjected to atomistic molecular dynamics simulations to refine the model and to probe the dynamics. After comparing to the wild type ACE2-RBD complex system, we found that the RBD^{O} exhibits stronger binding to human ACE2 protein, suggesting that the Omicron variant infects cells via the same mechanism and the infectivity might be enhanced due to the stronger binding interactions.

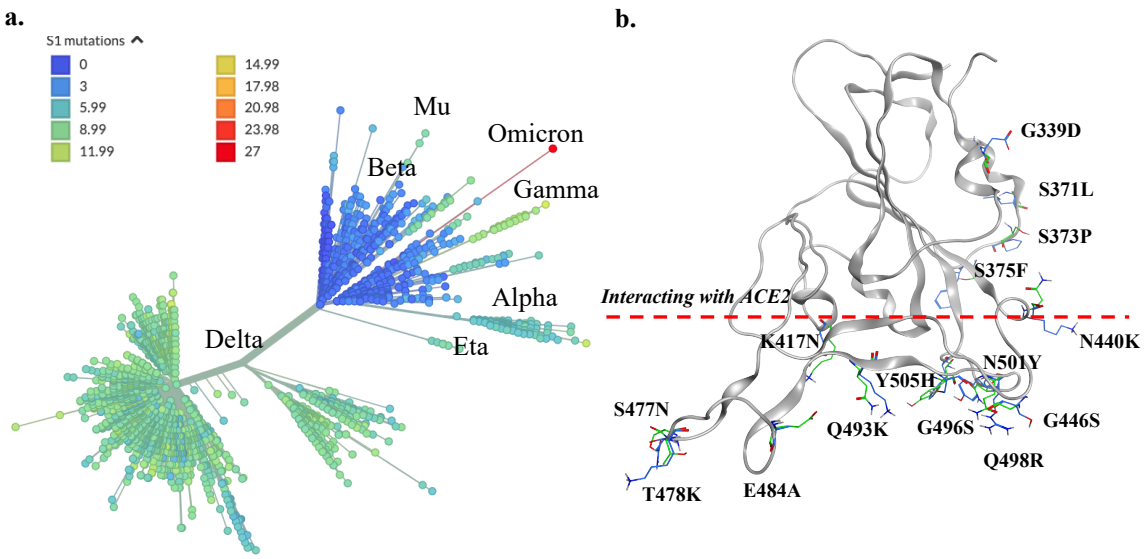

Figure 1. Mutations and the diversity of SARS-CoV-2. (**a**) The phylogenetic tree of SARS-CoV-2. Major variants are labelled on the graph, and the color of clans is according to the number of spike protein mutations. The tree is generated at https://nextstrain.org. (**b**) Mutation sites of the receptor binding domain. The residues below the red line are at or near the ACE2 binding interface.

Results

The structures of RBD and ACE2-RBD complex are stable. The averaged backbone root-mean-square-deviation (RMSD) of the RBD is less than 1.4 Å compared to the starting model (Figure 2a). For the wild type RBD, the structure ensembles from two

independent simulations (each 500 ns) deviated by 1.2 Å on average; interestingly, the RBD^O has averaged RMSD values of 1.4 Å, indicating that mutations only slightly alters the structure of RBD^O from the wild type RBD. Similarly, the ACE2-RBD complexes are stable from simulations, reflected on the RMSD with respect to starting complex structures (Figure 2b). The RMSD for the wild type ACE2-RBD complex are averaged to 3.0 Å and 2.5 Å in the structures sampled from the two trajectories; while the values are 2.2 Å and 2.6 Å for the two simulation trajectories of ACE2-RBD^O. Therefore, we predict that the mutations in Omicron variant do not significantly reduce the RBD stability, instead, the ACE2-RBD^O complex is even slightly more stable than the wild type complex according to the RMSD analysis. The residue fluctuations were analyzed by calculating the root-mean-square-fluctuations (RMSF) of the RBD (Figure 2c). According to the average values of RMSF, the RBD^O is more rigid than its wild type (1.5 Å vs. 2.1 Å). The reduction of the RMSF is more pronounced at the interfacing residues of RBD, also known as the receptor binding motif (RBD, residues 434-508) [17]. We also closely examined the flucutations of residues that were mutated (Figure 2c, right panel). We found that the 15 mutated residues in the Omicron variant consistently exhibit smaller fluctuations, compared to their wild type counterparts. It is plausible that the binding of ACE2 stabilize these residues, which in turn enhanced the stability of the ACE2-RBD^O complex. Detailed quantification on interactions between ACE2 and RBD are elaborated in the following sections.

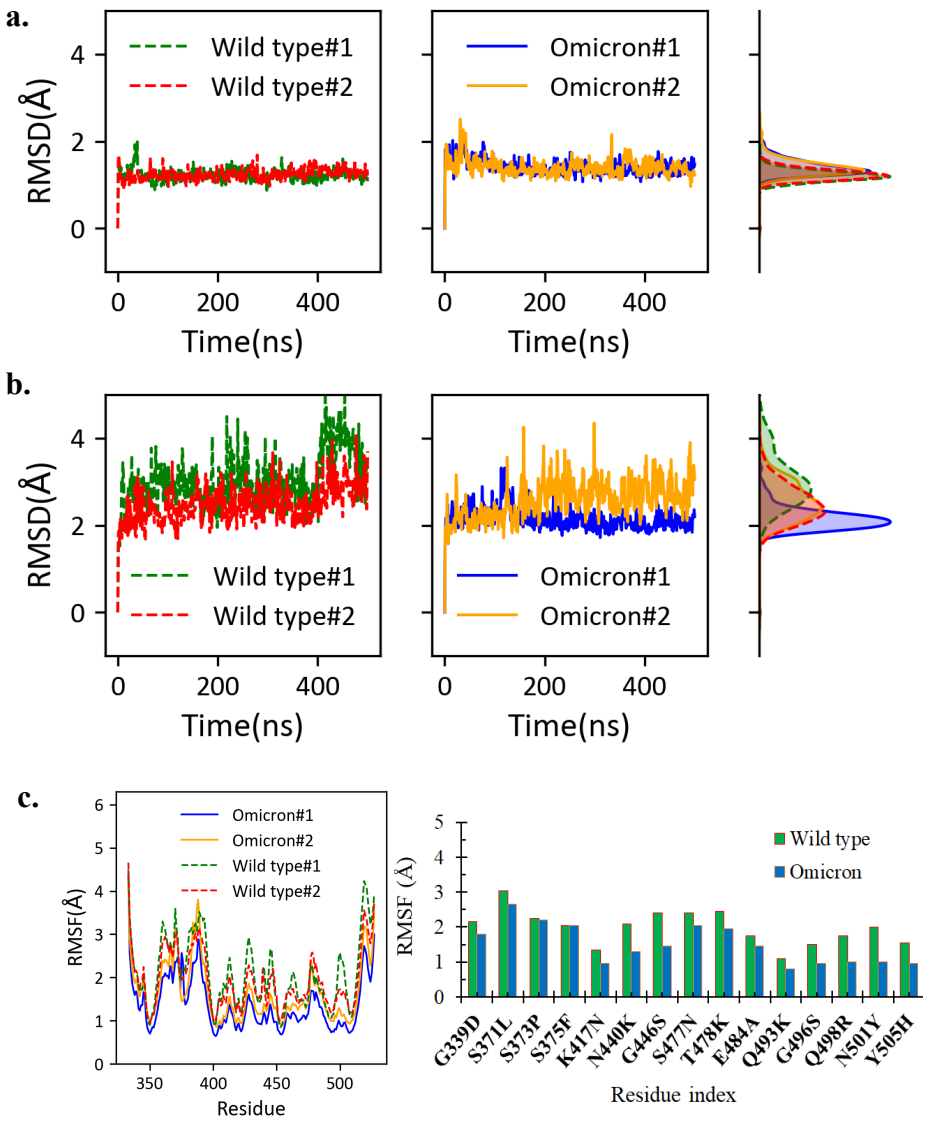

Figure 2. Stability of the RBD and ACE2-RBD complex structures. (**a**) The RMSD of RBD with respect to the starting structure. The histogram of each RMSD time trace is drawn on the right. (**b**) The RMSD of the whole complex with respect to the starting complex structure, with the histograms shown on the right. (**c**) The RBD residue fluctuations measured with RMSF. The residue fluctuations at the mutation sites are shown on the right.

The interactions between ACE2 and RBD is enhanced in Omicron variant. We extracted the hydrogen bonds formed directly between ACE2 and RBD^{O}, and further

compared to the wild type system (Figure 3). On average, there are 6.5 ± 2.2 hydrogen bonds formed between ACE2 and RBD^O, about 10% more than 5.9 ± 2.4 hydrogen bonds observed in the wild type system. A closer examination on the specific hydrogen bonds reveals that the Q493K and N501Y play important roles in forming new hydrogen bonds (Table 1). It is worthwhile to note that the hydrogen bonds are very dynamical, and the total number of hydrogen bonds at any instant time fluctuate significantly. Therefore, in the table we only listed seven hydrogen bonds that are frequently observed during simulations, with the occupancy near or above 20%. As shown in Table 1, only the hydrogen bond between ACE2 S19 and RBD A475 has an occupancy below 20% (18.73%). In the case of ACE2-RBDO, the next frequently observed hydrogen bond is between K31 of ACE2 and W456 of RBD^O with an occupancy of 16.25%. As shown in Table 1, there are five common stable hydrogen bonds observed in both the wild type and Omicron variant systems. The mutations resulted the loss of two hydrogen bonds: (1) the K417N mutation caused the loss of hydrogen bonding with ACE2 residue D30, and (2) the Y505H mutation significantly reduced its bonding to E37 of ACE2. The Q493K mutation maintains the hydrogen bond between Q493 and E35 of ACE2 in the wild type complex, adding the possibility of forming a new hydrogen bond between K493 and the D38 of ACE2. The hydrogen bond between Y501 of RBD^O and the Y41 of the ACE2 is also a new hydrogen bond frequently observed in simulations. The hydrogen bond between the S19 of ACE2 and the A475 of RBD^O is stronger than that in the wild type system, although neither residues were mutated in the Omicron variant. It is possibly influenced by the local changed due to the S477N and T478K mutations. By comparing the occupancies, we conclude that the hydrogen bonds between ACE2 and RBD^O is more stable through the simulations, and therefore resulting more hydrogen bonds on average.

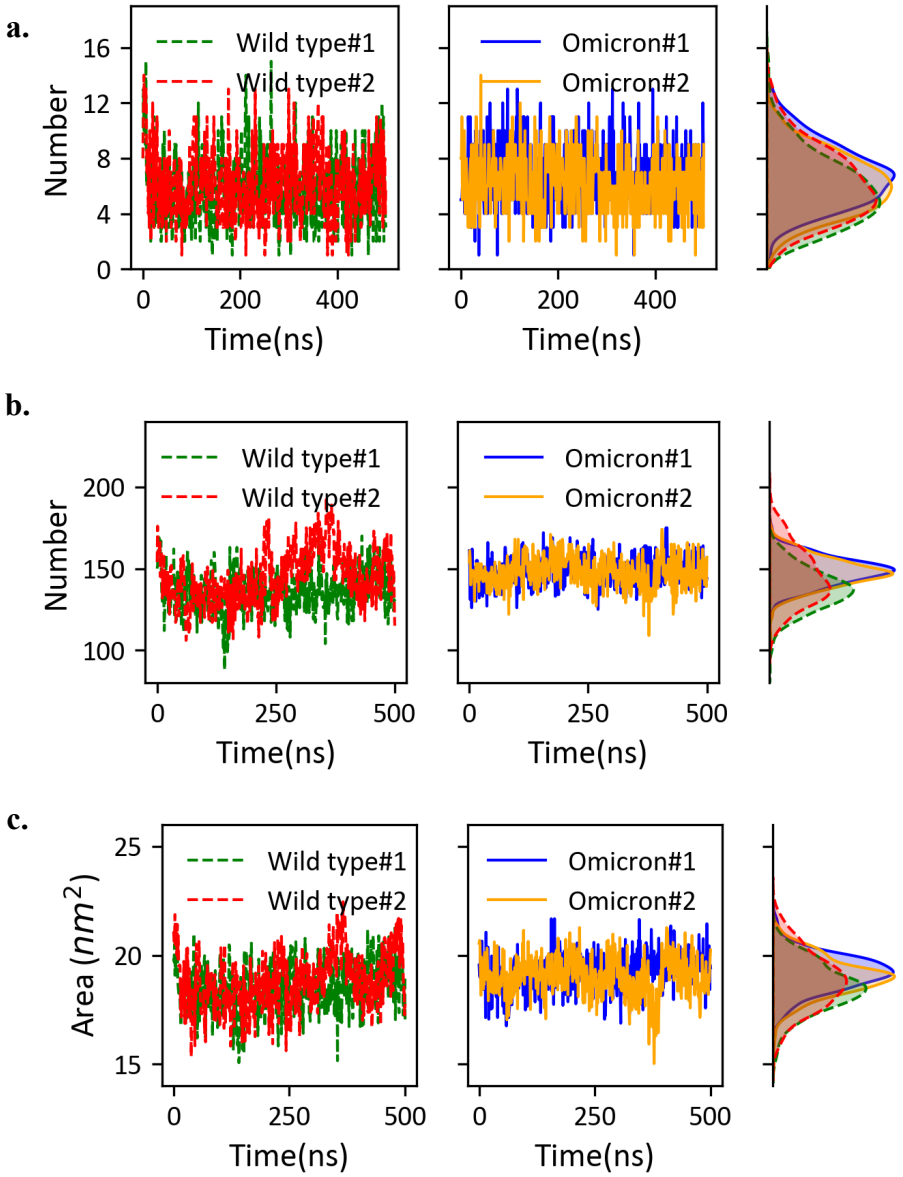

Figure 3. Quantitative analysis of the ACE2-RBD interactions. (**a**) Hydrogen bonds between ACE2 and RBD/RBD^{O}. The time traces of hydrogen bond numbers observed during the simulations. The histograms are shown on the right to compare the statistics between the wild type system and the Omicron variant system. (**b**) The number of residue contacts between ACE2 and RBD. (**c**) The buried surface area at the binding interface. Similar to (a), the histograms are shown to facilitate the comparison in (b,c).

140 **Table 1. Hydrogen bonds between the RBD and the ACE2.**

Wild type ACE2-RBD			Omicron ACE2-RBD		
ACE2	RBD	Occupancy	ACE2	RBD^O	Occupancy
K353-Main	G502-Main	57.97%	E35-Side	K493-Side *	75.67%
Y83-Side	N487-Side	50.60%	D355-Side	T500-Side	60.52%
E35-Side	Q493-Side	38.84%	K353-Main	G502-Main	57.03%
D30-Side	K417-Side	34.36%	D38-Side	K493-Side *	52.34%
D355-Side	T500-Side	25.60%	Y83-Side	N487-Side	52.04%
E37-Side	Y505-Side	21.71%	S19-Side	A475-Main	36.59%
S19-Side	A475-Main	18.73%	Y41-Side	Y501-Side *	35.00%

141 * The residue was mutated from the wild type RBD
142 The entries shaded in blue color are either not lost or with low occupancy in the Omicron variant
143 system; the entries with yellow shading are the new hydrogen bonds; the other entries are the
144 common hydrogen bonds.
145

146 We computed the number of van der Waals contacts between the ACE2 and RBD, as well
147 as the buried surface area, to further assess the binding affinity between ACE2 and RBD.
148 For the wild type system, the two simulations yields 137 ± 12 contacts on average, while
149 the ACE2-RBD^O has 148 ± 9 contacts on average (Figure 3b). The statistics on the buries
150 surface areas are consistent with the level of contacts. The Omicron variant resulted an
151 increase of buried surface area from 18.5 nm^2 to 19.1 nm^2 (Figure 3c).
152

153 **The representative structures are highly similar.** The representative structures were
154 selected from the most populated clusters for the ACE2-RBD complexes, in the wild type
155 and Omicron variant. The RBD structures are similar in the representative models, both
156 within 1.4 Å RMSD from the crystal structure (see Figure 4). In particular, the RBM
157 region are highly structurally consistent, in accordance with the tight binding to ACE2. We
158 computed the electrostatic potentials by solving the Poisson-Boltzmann equation for the
159 RBM region in three structures: the crystal structure and representative structure of the
160 wild type RBD, as well as the representative structure of the RBD^O. For the wild type
161 RBD, positive and negative potential patches are dispersively located at the binding
162 interface. Strikingly, the same interface has larger patches with positive potentials in the

RDB^{O}. For instance, the region centered around G446S-Q493K-G496S-Q498R-N501Y-Y505H mutation sites exhibits stronger positive electrostatic potentials, improving its complementary to the charge surface of ACE2 protein. In the corresponding region, the key residues from ACE2 is composed of D38-Y41-Q42-D355-S446, forming a negatively charged patch (Figure 4c). We computed the binding energies for the representative models. In this case, we obtained a representative structure from each simulation trajectory using the same clustering algorithm, e.g., two for the wild type ACE-RBD, and two for the Omicron variant system. The binding energies for the two wild type ACE2-RBD structures are -104.17 kcal/mol and -97.73 kcal/mol. The binding energies for ACE2-RBD^{O} structures have lower values (-112.25 kcal/mol and -107.04 kcal/mol), indicating stronger binding between ACE2 and RBD^{O}.

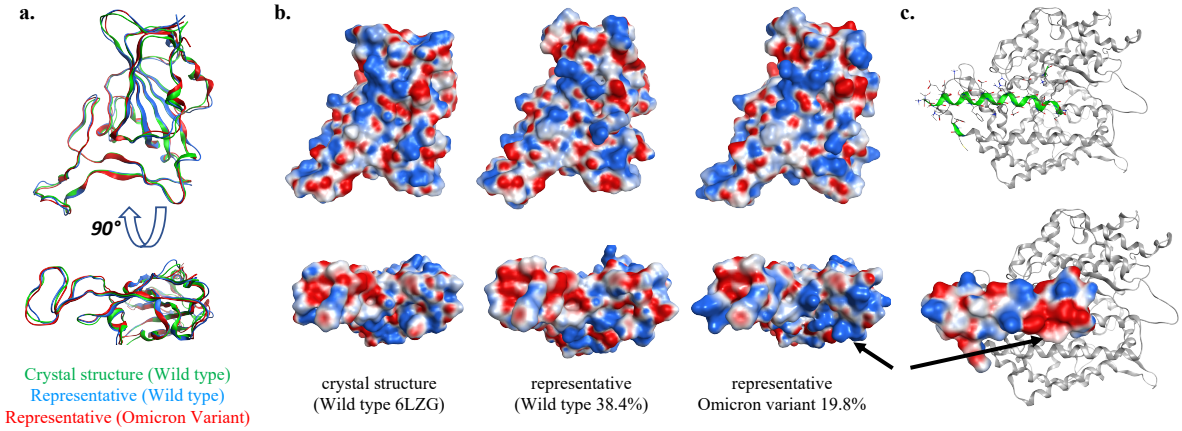

Figure 4. Representative structures and the electrostatic potential surfaces. (**a**) The representative structures of wild type RBD (blue) and RBD^{O} (red) are superposed to the crystal structure (green). The bottom panel shows the RBD binding interface to ACE2. (**b**) The electrostatic potentials on the RBD/RBD^{O} surface. (**c**) The RBD binding interface of ACE2 and its electrostatic potentials (crystal structure of ACE2). The black arrows point to the positive and negative potential patches.

Detailed structure features at the interface

The interactions at the interface of ACE2-RBD complex for the wildtype have been previous reported for both the crystal structures [18,19] and the dynamic conformations from computational simulations [13]. Generally, ACE2 residues 19-42 of the N-terminal helix, 82-83 near the η1, N330 at helix-13 and 352-357 at the β-hairpin-4,5 are known to be interacting with RBD. For the RBD, crystal structures show residues K417, G446, Y449, Y453, L455, F456, A475, F486, N487, Y489, Q493, Y495, G496, Q498, T500, N501, G502 and Y505 interacting with hACE2, while simulations have reported additional residues Q474, G476, S477, T478 , E484 and G485 all at the loop (L67) of RBD to enhance the interactions. Out of the 15 RBD mutations found in the omicron variant, 10 residues (K417N, N440K, G446S, S477N, T478K, E484A, Q493K, G496S, Q498R, N501Y and Y505H) are located at interface, consequently changing the electrostatics surface charges at the interface and may have additional effects on the binding of antibodies and drugs targeting the interface due to the bulkier size of the mutant sidechains such as in T478K. This also applies for the mutant residue N400K at a loop near the binding interface with ACE2.

As a result of these mutations, wildtype RBD-ACE2 interactions (Figure 5) such as salt bridge E484-K31 are lost , K417-D30 are weakened in the Omicron variant due to shortened side chain, while hydrogen bonds Q493-E35, Q498-K353, Y505-E37 are enhanced by substitutions, repositioning and formation of new interactions, K493-D38, R498-Y41, R498-Q42 H505-K353 and N377-Q24 respectively and by supplementing with additional π-π stacking interaction Y501-Y41. The rest of interactions observed in wildtype ACE2-RBD (e.g., hydrogen bonds and contacts between Y449-D38, Y453-H34 A475-S19, N487-Y83, T500-N330 and T500-D355) are also maintained in the omicron variant (Figure 5).

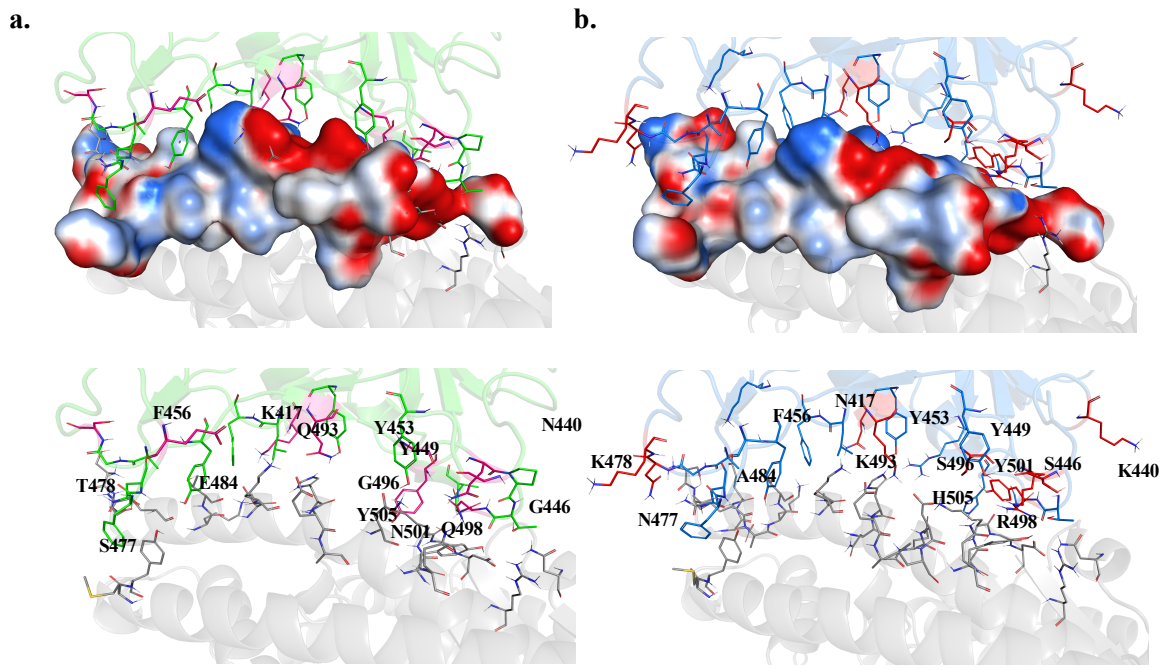

Figure 5. The detailed structure at the ACE2-RBD binding interface. (**a**) the interface of the wild type ACE2-RBD complex, the amino acids at mutation sites are shown with stick representations.. The upper panels shows the side chain positions of RBD on the surface of ACE2, where the surface is colored according to electrostatic potentials (blue for positive and red for negative potentials); lower panel shows the side chains of both ACE2 and RBD. (**b**) the interactions between ACE2-RBDO of the Omicron variant. The figure labeling and coloring scheme are the same as in (a), except residues are the mutated.

Discussions and Conclusion

The large number of mutations observed in the spike protein of SARS-CoV-2 raised serious concerns about the new variant Omicron. Using computational modeling and simulations, we carried out quantitative analysis on the stability of ACE2-RBD complex for the Omicron variant, and compared to that of the wild type system. The interactions are assessed using several quantities, including hydrogen bonding, van der Waals contacts, buried surface areas, and the binding free energies. The dynamics simulation results and the quantitative comparison show that the binding interactions between ACE2 and RBD are slightly stronger for the Omicron variant than for the wild type. This information

provides molecular basis for enhanced infectivity of the Omicron variant. For antibodies targeting the RBD at the ACE2 binding interface, the efficacy might not be influenced by the mutation. The study also confirms that the ACE2 can still serve as the receptor for Omicron variant, despite the large number of mutations.

Methods

Molecular Dynamics Simulation and Analysis

The mutation information of Omicron is retrieved from the US CDC website [9]. We included 15 mutations occurred in the RDB (see Figure 1). The mutations were implemented based on the wild type ACE2-RBD complex structure using the Charmm-GUI webserver [20]. The protonation state was determined under PH 7.0 solvent environment.

The wild type ACE2-RBD and its Omicron variant were prepared using the CHARMM36 force fields, following the procedure of the CHARMM-GUI webserver. Each system was solvated in 150 mM sodium chloride solvent with TIP3P water models. Steepest descent algorithm was applied to minimize the system energy, then each system was equilibrated to 310.15 K (37 °C) within 125 ps. The temperature was maintained by Nose-Hoover scheme with 1.0 ps coupling constant in the NVT ensemble (constant volume and temperature). During the equilibration stage, harmonic restraint forces were applied to the molecules (400 kJ mol^{-1} nm^{-2} on backbone and 40 kJ mol^{-1} nm^{-2} on the side chain atoms) [21,22]. Subsequently, the harmonic restraints were removed and the NPT ensembles (constant pressure and temperature) were simulated at one atmosphere pressure (10^5 Pa) and 310.15 K. The pressure was maintained by isotropic Parrinello-Rahman barostat [23], with a compressibility of 4.5×10^{-5} bar^{-1} and a coupling time constant of 5.0 ps. The wild type and Omicron variant ACE2-RBD systems were both simulated for 2 x 500 ns using the

GROMACS 5.1.2 package [24]. In all simulations, a time step of 2.0 fs was used and the PME (particle mesh Ewald) [25] was applied for electrostatic interactions beyond 12.0 Å. The van der Waals interaction cutoff was set to 12.0 Å. Hydrogen atoms were constrained using the LINCS algorithm [26].

Analyses were carried out with tools in GROMACS (rmsd, rmsf, mindist, sasa) to examine the system stability. The buried surface area is computed as

$$\Delta A = A_{ACE2} + A_{RBD} - A_{ACE2\text{-}RBD} \qquad (1)$$

Where A_{ACE2}, A_{RBD}, and $A_{ACE2\text{-}RBD}$ are the solvent accessible surface area computed using gmx sasa function. The mindist command was used to compute the residue distances, the residue pairs with distance below 4.0 Å were considered as contacting residues.

VMD was used to analyze hydrogen bonding interactions [27], with the following criteria: D-A distance cutoff=3.9 Å and D-H-A angle cutoff=20 degrees, where D,A,H are Donor atom, Acceptor atom, and the Hydrogen atom linked to the Donor atom. Pymol was used for molecular binding interface, water distributions, visualization, and rending model images [27]. The adaptive Poisson-Boltzmann equation solver (APBS) was used to compute the electrostatic potentials [28].

The binding energy was calculated using Prime 3.0 MM-GBSA module of the Schrodinger 24 package . In each ACE2-RBD complex, the ACE2 was treated as the receptor and RBD was considered as the ligand. Prime MM-GBSA uses OPLS-AA force field and VSGB 2.0 implicit solvation model to estimate the binding energy of the receptor-ligand complex. The binding energy is calculated as:

$$\Delta G\ (\text{bind}) = E_{ACE2\text{-}RBD} - (E_{ACE2} + E_{RBD}) \qquad (2)$$

Acknowledgement

Funding from National Natural Science Foundation of China (grant numbers: U1930402, 31971136). The work is supported by a Tianhe-2JK computing time award at Beijing Computational Science Research Center (CSRC).

Competing interests

The authors declare no competing interests.

Reference:

[1] I. Ishigami, N.A. Zatsepin, M. Hikita, C.E. Conrad, G. Nelson, J.D. Coe, S. Basu, T.D. Grant, M.H. Seaberg, R.G. Sierra, M.S. Hunter, P. Fromme, R. Fromme, S.R. Yeh, D.L. Rousseau, Crystal structure of CO-bound cytochrome c oxidase determined by serial femtosecond X-ray crystallography at room temperature, Proc. Natl. Acad. Sci. U. S. A. 114 (2017) 8011–8016. https://doi.org/10.1073/pnas.1705628114.

[2] Johns Hopkins Coronavirus Resource Center, (n.d.). https://coronavirus.jhu.edu/vaccines/vaccines-faq (accessed December 6, 2021).

[3] E. Mathieu, H. Ritchie, E. Ortiz-Ospina, M. Roser, J. Hasell, C. Appel, C. Giattino, L. Rodés-Guirao, A global database of COVID-19 vaccinations, Nat. Hum. Behav. 5 (2021) 947–953. https://doi.org/10.1038/s41562-021-01122-8.

[4] J.S. Tregoning, K.E. Flight, S.L. Higham, Z. Wang, B.F. Pierce, Progress of the COVID-19 vaccine effort: viruses, vaccines and variants versus efficacy, effectiveness and escape, Nat. Rev. Immunol. 2021 2110. 21 (2021) 626–636. https://doi.org/10.1038/s41577-021-00592-1.

[5] P.R. Krause, T.R. Fleming, R. Peto, I.M. Longini, J.P. Figueroa, J.A.C. Sterne, A. Cravioto, H. Rees, J.P.T. Higgins, I. Boutron, H. Pan, M.F. Gruber, N. Arora, F. Kazi, R. Gaspar, S. Swaminathan, M.J. Ryan, A.M. Henao-Restrepo, Considerations in boosting COVID-19 vaccine immune responses, Lancet. 398 (2021) 1377–1380. https://doi.org/10.1016/S0140-6736(21)02046-8/ATTACHMENT/99B4689E-FA37-476A-B30E-8D1E3B4E33BC/MMC1.PDF.

[6] A.P. Vashi, O.C. Coiado, The future of COVID-19: A vaccine review, J. Infect. Public Health. 14 (2021) 1461–1465. https://doi.org/10.1016/J.JIPH.2021.08.011.

[7] L. Wang, T. Zhou, Y. Zhang, E.S. Yang, C.A. Schramm, W. Shi, A. Pegu, O.K. Oloniniyi, A.R. Henry, S. Darko, S.R. Narpala, C. Hatcher, D.R. Martinez, Y. Tsybovsky, E. Phung, O.M. Abiona, A. Antia, E.M. Cale, L.A. Chang, M. Choe, K.S. Corbett, R.L. Davis, A.T. DiPiazza, I.J. Gordon, S.H. Hait, T. Hermanus, P. Kgagudi, F. Laboune, K. Leung, T. Liu, R.D. Mason, A.F. Nazzari, L. Novik, S. O'Connell, S. O'Dell, A.S. Olia, S.D. Schmidt, T. Stephens, C.D. Stringham, C.A. Talana, I.T. Teng, D.A. Wagner, A.T. Widge, B. Zhang, M. Roederer, J.E. Ledgerwood, T.J. Ruckwardt, M.R. Gaudinski, P.L. Moore, N.A. Doria-Rose, R.S. Baric, B.S. Graham, A.B. McDermott, D.C. Douek, P.D. Kwong, J.R. Mascola, N.J. Sullivan, J. Misasi, Ultrapotent antibodies against diverse and highly transmissible SARS-CoV-2 variants, Science. 373 (2021). https://doi.org/10.1126/science.abh1766.

[8] Classification of Omicron (B.1.1.529): SARS-CoV-2 Variant of Concern, (n.d.). https://www.who.int/news/item/26-11-2021-classification-of-omicron-(b.1.1.529)-sars-cov-2-variant-of-concern (accessed December 9, 2021).

[9] Science Brief: Omicron (B.1.1.529) Variant | CDC, (n.d.). https://www.cdc.gov/coronavirus/2019-ncov/science/science-briefs/scientific-brief-omicron-variant.html (accessed December 9, 2021).

[10] J. Shang, G. Ye, K. Shi, Y. Wan, C. Luo, H. Aihara, Q. Geng, A. Auerbach, F. Li, Structural basis of receptor recognition by SARS-CoV-2, Nature. 581 (2020) 221–224. https://doi.org/10.1038/s41586-020-2179-y.

[11] R. Yan, Y. Zhang, Y. Li, L. Xia, Y. Guo, Q. Zhou, Structural basis for the recognition of SARS-CoV-2 by full-length human ACE2, Science. 367 (2020) 1444–1448. https://doi.org/10.1126/science.abb2762.

[12] Y. Wang, M. Liu, J. Gao, Enhanced receptor binding of SARS-CoV-2 through networks of hydrogen-bonding and hydrophobic interactions, Proc. Natl. Acad. Sci. 117 (2020) 13967–13974. https://doi.org/10.1073/pnas.2008209117.

[13] C.S. Lupala, X. Li, J. Lei, H. Chen, J. Qi, H. Liu, X.-D. Su, Computational simulations

reveal the binding dynamics between human ACE2 and the receptor binding domain of SARS-CoV-2 spike protein, Quant. Biol. 9 (2021) 61. https://doi.org/10.15302/J-QB-020-0231.

[14] X. Xu, P. Chen, J. Wang, J. Feng, H. Zhou, X. Li, W. Zhong, P. Hao, Evolution of the novel coronavirus from the ongoing Wuhan outbreak and modeling of its spike protein for risk of human transmission, Sci. China Life Sci. 63 (2020) 457–460. https://doi.org/10.1007/s11427-020-1637-5.

[15] J. Damas, G.M. Hughes, K.C. Keough, C.A. Painter, N.S. Persky, M. Corbo, M. Hiller, K.P. Koepfli, A.R. Pfenning, H. Zhao, D.P. Genereux, R. Swofford, K.S. Pollard, O.A. Ryder, M.T. Nweeia, K. Lindblad-Toh, E.C. Teeling, E.K. Karlsson, H.A. Lewin, Broad host range of SARS-CoV-2 predicted by comparative and structural analysis of ACE2 in vertebrates, Proc. Natl. Acad. Sci. U. S. A. 117 (2020) 22311–22322. https://doi.org/10.1073/pnas.2010146117.

[16] C.S. Lupala, V. Kumar, X. Su, C. Wu, H. Liu, Computational insights into differential interaction of mammalian angiotensin-converting enzyme 2 with the SARS-CoV-2 spike receptor binding domain, Comput. Biol. Med. (2021) 105017. https://doi.org/10.1016/j.compbiomed.2021.105017.

[17] C. Yi, X. Sun, J. Ye, L. Ding, M. Liu, Z. Yang, X. Lu, Y. Zhang, L. Ma, W. Gu, A. Qu, J. Xu, Z. Shi, Z. Ling, B. Sun, Key residues of the receptor binding motif in the spike protein of SARS-CoV-2 that interact with ACE2 and neutralizing antibodies, Cell. Mol. Immunol. 17 (2020) 621–630. https://doi.org/10.1038/s41423-020-0458-z.

[18] Q. Wang, Y. Zhang, L. Wu, S. Niu, C. Song, Z. Zhang, G. Lu, C. Qiao, Y. Hu, K.Y. Yuen, Q. Wang, H. Zhou, J. Yan, J. Qi, Structural and Functional Basis of SARS-CoV-2 Entry by Using Human ACE2, Cell. 181 (2020) 894-904.e9. https://doi.org/10.1016/j.cell.2020.03.045.

[19] J. Lan, J. Ge, J. Yu, S. Shan, H. Zhou, S. Fan, Q. Zhang, X. Shi, Q. Wang, L. Zhang, X. Wang, Structure of the SARS-CoV-2 spike receptor-binding domain bound to the ACE2 receptor., Nature. (2020). https://doi.org/10.1038/s41586-020-2180-5.

[20] J. Lee, X. Cheng, J.M. Swails, M.S. Yeom, P.K. Eastman, J.A. Lemkul, S. Wei, J. Buckner, J.C. Jeong, Y. Qi, S. Jo, V.S. Pande, D.A. Case, C.L. Brooks, A.D. MacKerell, J.B. Klauda, W. Im, CHARMM-GUI Input Generator for NAMD, GROMACS, AMBER, OpenMM, and CHARMM/OpenMM Simulations Using the CHARMM36 Additive Force Field, J. Chem. Theory Comput. 12 (2016) 405–413. https://doi.org/10.1021/acs.jctc.5b00935.

[21] S. Nosé, A unified formulation of the constant temperature molecular dynamics methods, J. Chem. Phys. 81 (1984) 511–519. https://doi.org/10.1063/1.447334.

[22] W.G. Hoover, Canonical dynamics: Equilibrium phase-space distributions, Phys. Rev. A. 31 (1985) 1695–1697. https://doi.org/10.1103/PhysRevA.31.1695.

[23] M. Parrinello, A. Rahman, Polymorphic transitions in single crystals: A new molecular dynamics method, J. Appl. Phys. 52 (1981) 7182–7190. https://doi.org/10.1063/1.328693.

[24] M.J. Abraham, T. Murtola, R. Schulz, S. Páll, J.C. Smith, B. Hess, E. Lindah, Gromacs: High performance molecular simulations through multi-level parallelism from laptops to supercomputers, SoftwareX. 1–2 (2015) 19–25. https://doi.org/10.1016/j.softx.2015.06.001.

[25] T. Darden, D. York, L. Pedersen, Particle mesh Ewald: An N·log(N) method for Ewald sums in large systems, J. Chem. Phys. 98 (1993) 10089–10092. https://doi.org/10.1063/1.464397.

[26] B. Hess, H. Bekker, H.J.C. Berendsen, J.G.E.M. Fraaije, LINCS: A Linear Constraint Solver for molecular simulations, J. Comput. Chem. 18 (1997) 1463–1472.

https://doi.org/10.1002/(SICI)1096-987X(199709)18:12<1463::AID-JCC4>3.0.CO;2-H.

[27] W. Humphrey, A. Dalke, K. Schulten, VMD: Visual molecular dynamics, J. Mol. Graph. 14 (1996) 33–38. https://doi.org/10.1016/0263-7855(96)00018-5.

[28] E. Jurrus, D. Engel, K. Star, K. Monson, J. Brandi, L.E. Felberg, D.H. Brookes, L. Wilson, J. Chen, K. Liles, M. Chun, P. Li, D.W. Gohara, T. Dolinsky, R. Konecny, D.R. Koes, J.E. Nielsen, T. Head-Gordon, W. Geng, R. Krasny, G.W. Wei, M.J. Holst, J.A. McCammon, N.A. Baker, Improvements to the APBS biomolecular solvation software suite, Protein Sci. 27 (2018) 112–128. https://doi.org/10.1002/pro.3280.

Supporting Information